HERON is jointly edited by:
STEVIN-LABORATORY of the department of Civil Engineering, Delft University of Technology, Delft, The Netherlands
and
INSTITUTE TNO for Building Materials and Building Structures, Rijswijk (ZH), The Netherlands.
HERON contains contributions based mainly on research work performed in these laboratories on strength of materials, structures and materials science.

Secretary:
G. J. van Alphen
Stevinweg 1
P.O. Box 5048
2600 GA Delft, The Netherlands
Tel. 0031-15-785919
Telex 38070 BITHD

HERON vol. 29 1984 no. 2

Contents

FRACTURE MECHANICS OF AN ELASTIC SOFTENING MATERIAL LIKE CONCRETE

H. W. Reinhardt
Delft University of Technology
Department of Civil Engineering
Stevin Laboratory
Stevinweg 4, P.O. Box 5048, 2600 GA Delft, The Netherlands

FRACTURE MECHANICS OF AN ELASTIC SOFTENING MATERIAL LIKE CONCRETE

Summary

Concrete is modelled as a linear elastic softening material and introduced into fracture mechanics. A discrete crack is considered with softening zones at the crack tips. Following the approach of Dugdale/Barenblatt, closing stresses are applied to the crack faces in the softening zone. The stresses are described by a power function. Relations are worked out between the remote stress on a cracked plate, the tensile strength of the material and the size of the softening zone. The finite width of a plate is considered and so are various stress distributions of the softening zone.

Experiments were performed to estabilish the stress-strain behaviour of concrete in deformation-controlled uniaxial tensile loading. Furthermore, it was investigated whether cyclic loading affects the static envelope curve. A qualitative model is presented which illustrates the effect of prepeak cyclic loading on deformation and stress distribution in a specimen.

The results show that nonlinear fracture mechanics can be applied to concrete. The loadbearing capacity of a cracked plate can be predicted with reasonable accuracy. As appears from the experiments, the application of this approach to cyclic loading is very promising.

Fracture mechanics of an elastic softening material like concrete

1 Introduction

During the last two decades much effort has been devoted to developing advanced methods for the analysis of concrete structures [14]. Numerical techniques have been so improved that complicated structures under complex loadings could be dealt with, as exemplified by finite element methods capable of analysing concrete offshore structures under dynamic, thermal and hydrostatic forces [15]. With the development of these methods the demand for correct material models grew enormously. Models have been derived for the multiaxial behaviour of concrete under compression, for impact loading, for creep and shrinkage and other phenomena. The specialists realized that the tensile behaviour of concrete should be given more attention than before [16, 17]. Usually the tensile strength of concrete is neglected in engineering analysis although it is well known that bending shear, punching shear and bond capacity rely on the tensile properties of concrete. Since tensile behaviour and cracking are interrelated it was not surprising that fracture mechanics entered the scene.

On the other hand, materials testing proceeded steadily with advanced methods. Deformation-controlled testing became feasible also for brittle materials thanks to electronically controlled testing equipment. Uniaxial tensile tests could be carried out according to a predetermined loading or deformation pattern [18]. Fatigue of concrete has been studied extensively in compression, in tension, and in alternating tension-compression loading.

It is now the time to combine the two approaches - theoretical modelling and materials testing - in order to gain more insight into the physical behaviour and to verify the knowledge as applied to a real material. The aim of this study is to extend nonlinear fracture mechanics to the specific features of concrete and to use experiments for input of correct data and for verification of results. At this moment the analytical model will be confined to static loading, whereas the experiments will moreover provide data for cyclic loading. In the near future these data will be used for setting up a fatigue model for concrete.

In this study concrete will be treated as a linear elastic softening material, which means that a tensile specimen exhibits a linear stress-strain curve until maximum stress is reached (which is called tensile strength) and that thereafter the stress decays with increasing deformation. After the top of the stress-strain-curve has been reached, "strain" is no longer the correct term, since a crack will form which opens up while the remainder of the specimen unloads elastically (without permanent strain). So, beyond the top, deformation is composed of the remaining elastic strain ($\varepsilon = \sigma/E$) and the differential displacement of the crack faces. The crack is conceived as discrete, though in reality a concrete crack is certainly not one discrete line. It starts as a microcracking

zone and its deformation is finally concentrated in one discrete crack. For modelling purpose the assumption of one crack is advantageous, however.

Ideally, the stress-deformation behaviour should be studied on small homogeneous uncracked specimens. But it is well known that concrete contains tiny flaws and inhomogeneities from the beginning. What is measured on concrete is already an average behaviour of a flawed material and this is modelled as a linear elastic softening material. On the other hand, large specimens or structural members show visible cracks which should be treated by an appropriate method. In this study fracture mechanics will be used.

2 Modelling of the crack tip zone

2.1 *Stresses and softening zone size*

Nonlinear fracture mechanics will be used to model the stress and deformation behaviour near a crack. According to the approach of Dugdale [1] and Barenblatt [2] the crack is subdivided into two parts: a part where the crack faces are traction free and a part where a closing stress acts along the cracks faces. The first part extends along 2a in Fig. 1 and the second is represented by the two areas $(c-a)$. The total crack has the length 2c. In the case of an elastic-plastic material the crack closing stress is equal to the yield stress. In a strain-hardening material the stress distribution depends on the hardening coefficient and the crack tip deformation [3]. Since concrete is a strain softening material [4] the stress distribution is a function of the deformation and the softening behaviour.

The simplest case of a central crack in an infinite sheet of concrete will be considered. A remote normal stress σ causes a stress and strain distribution near the crack tip which is - in the case of a linear elastic material - determined by the stress intensity factor

$$K_\sigma = \sigma\sqrt{\pi c} \tag{1}$$

and a function expressed in r and θ, which are polar co-ordinates with their origin at the crack tip. For $\theta = 0$ the normal stress distribution is given by

$$\sigma(r) = \frac{K_\sigma}{\sqrt{2\pi r}} \tag{2}$$

Eq. (2) shows a singularity at $r = 0$. Since stresses cannot grow to infinity, yielding will take place in a plastic material or softening will start in a softening material. Dugdale calculated the size of the plasticized zone from the condition that the same stress intensity factor should be developed by the crack closing stresses at the crack tip as due to the remote stress. For an arbitrary stress distribution $p(t)$ within the region $(c-a)$ the stress intensity factor is given by [5]

$$K_p = 2\sqrt{c/\pi} \int_a^c \frac{p(t)\,\mathrm{d}t}{\sqrt{c^2 - t^2}} \tag{3}$$

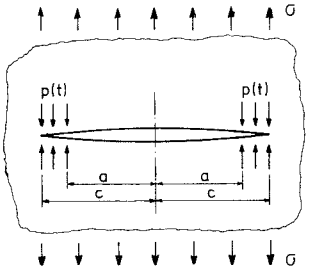

Fig. 1. Crack geometry.

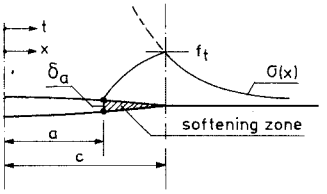

Fig. 2. Stresses in softening zone and crack tip opening displacement δ_a.

Equating K_σ and K_p leads to an expression for the size of the plastic zone $(c-a)$ depending on the stress $p(t)$.

Whereas for a plastic material $p(t) = \text{const.}$, the stress distribution in a softening material is not known in advance. It is a function of the stress deformation curve and the deformation of the crack tip. In order to model concrete by this approach, a simple function will be adopted for the stress distribution in the softening zone. Later on it will be verified by experiments.

From Fig. 2 it is obvious that the maximum stress that occurs is the tensile strength of concrete. Between the tip of the softening zone $x = c$ and the tip of the visible crack $x = a$ the deformation exceeds the elastic limit, which means a stress release according to the softening behaviour of the material. In this study the stress distribution within the softening zone will be described by the power function

$$\frac{p(t)}{f_t} = 1 - \left(\frac{c-t}{c-a}\right)^n \tag{4}$$

Fig. 3 shows this stress distribution with n as the parameter. A small value of n indicates a steep reduction of stress whereas with a large value of n there is still considerable stress transfer in the softening zone. $n \to \infty$ leads to Dugdale's elastic-plastic case.

Eq. (4) contains the condition that at the beginning of the softening zone, at $x = a$, the

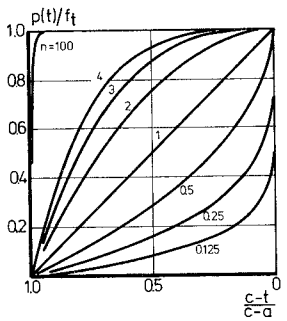

Fig. 3. Stresses in a complete softening zone with exponent n as a parameter.

stress is zero. This is not necessarily true. This is only valid if the deformation of the softening zone at $x = a$ is equal to the limiting value δ_0 of the stress deformation curve as indicated by Fig. 4. Usually a crack starts from zero crack width. Increasing stress leads to an increase of the crack width which finally reaches the limiting value δ_0. Later on it will be shown that a certain minimum crack length is necessary in order to develop a complete crack softening zone. Therefore a modification of eq. (4) will be used, which reads

$$\frac{p(t)}{f_t} = 1 - \gamma \left(\frac{c-t}{c-a}\right)^n \tag{5}$$

where γ is a factor between 1 and 0. $\gamma = 1$ means a complete stress release at $x = a$ and $\gamma = 0$ means no reduction of stress at all. Fig. 5 illustrates the case where $\gamma = 0{,}5$.

γ can be characterised by

$$\gamma = 1 - p_{t=a}/f_t \tag{6}$$

For a general treatment, n and γ are to be regarded as independent parameters.

Combination of eq. (3) and eq. (5) leads to

$$K_p = 2f_t\sqrt{c/\pi} \int_a^c \frac{1 - \gamma \left(\frac{c-t}{c-a}\right)^n}{\sqrt{c^2 - t^2}}\, dt \tag{7}$$

which should be equated with eq. (1) in order to make the stress singularity at $x = c$ vanish. After eq. (7) has been solved by numerical integration, the result can be shown as a relation between $\beta = a/c$ and σ/f_t with n and γ as parameters.

Fig. 6 is a set of four diagrams for $n = 0{,}125, 0{,}25, 0{,}5, 1, 2, 4, 100$ and $\gamma = 1, 0{,}75, 0{,}50, 0{,}25$, respectively. Several features will be discussed. The vertical axis of the diagram gives $\beta = a/c$, which is a measure of the size of the softening zone. A large value of β means a small softening zone while a small value of β means that c has grown considerably in relation to a. $\beta = 0$ can be interpreted as a failure criterion since $c \to \infty$ for a constant value of a leads to complete softening of the whole cross-section. The remote

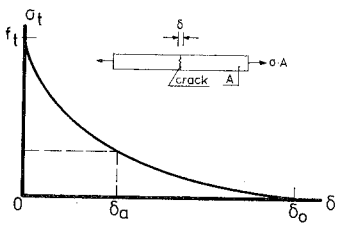

Fig. 4. Stress vs. crack opening.

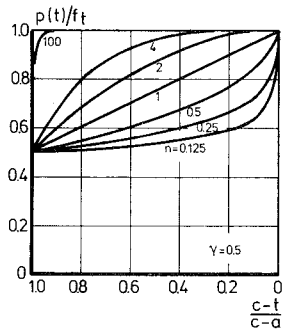

Fig. 5. Stresses in a softening zone with $\gamma = 0{,}5$.

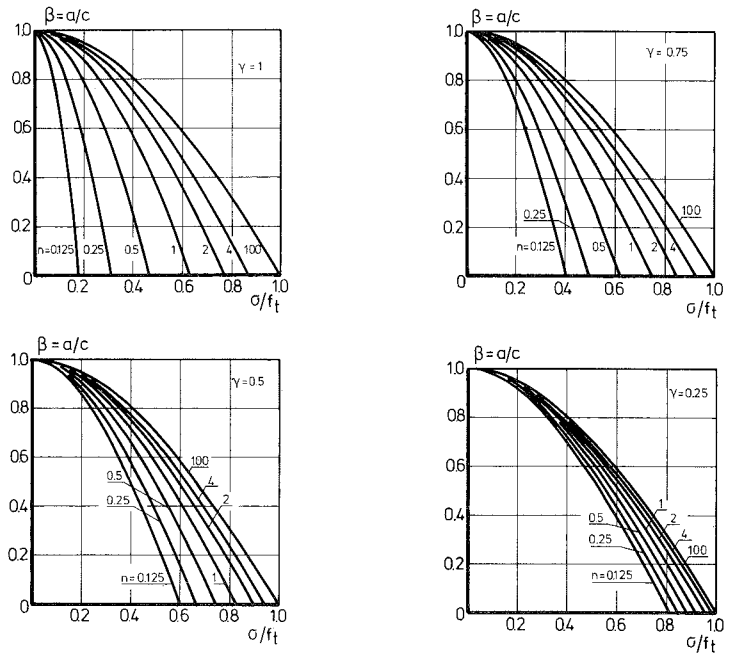

Fig. 6. Size of softening zone vs. remote stress for various n and
a. $\gamma = 1$
b. $\gamma = 0{,}75$
c. $\gamma = 0{,}50$
d. $\gamma = 0{,}25$.

stress σ divided by the uniaxial tensile strength f_t is plotted along the horizontal axis. Thus, the lines describe the extent of the softening zone for given values of n and γ. Consider for example $\gamma = 1$ (Fig. 6a) and $n = 0{,}5$. For a stress-strength ratio of 0,2, β becomes 0,78, which means that the extension of the softening zone in relation to the original crack $(c-a)/a$ is equal to 0,28. If σ/f_t is taken as 0,4, β becomes 0,24 and $(c-a)/a$ is then 3,17. The softening zone has already exceeded the original crack length. For $n = 0{,}5$ and $\beta = 0$ σ/f_t is 0,47, which means that the maximum attainable stress in a cracked plate is only 0,47 times the strength of an uncracked material. For $\gamma = 1$ the influence of the power n on the softening zone in relation to the stress is very strong. A low value of n considerably reduces β already at small stresses, whereas a high value of n delays softening. $n = 100$ shows that $\beta = 0$ is reached only when $\sigma = f_t$, which was to be expected.

In comparison with $\gamma = 1$, lower values of γ reduce the influence of n in a relative and an absolute sense. As can be seen from Fig. 6d, the lines shift to the right, while the line farthest to the right remains almost unaffected. The difference between $n = 0{,}125$ and $n = 100$ has become small. For the same conbination as above ($n = 0{,}5$, $\sigma = 0{,}4 f_t$) β is 0,74 or $(c-a)/a$ is 0,35, as compared with 3,17 above. The stress at which failure occurs ($\beta = 0$) is now $0{,}88 f_t$ as compared with 0,47. This means that the attainable stress

is higher if the stress at the tip of the visible crack does not decrease so much. Of course, this result was to be expected in a qualitative sense.

The information contained in Fig. 6 can be evaluated in two other ways, namely, in regard to strength or in regard to softening zone size. The first question is: what is the influence of n on the maximum attainable stress? Since there is no condition stated in respect to original crack length, even a small crack may lead to failure if the softening zone spreads over the whole cross-section. A limiting case is the tensile test of a specimen when (tiny) cracks are present but not mentioned. The maximum stress is usually called the strength f_t. In reality this so-called strength has been influenced by cracks and is only an apparent strength. The real strength is higher. It should be a function of n, since small n spreads the softening zone already at low stresses. The real strength f^* can be defined as follows:

$$f^*/f_t = f_t/\sigma$$

For $\beta = 0$ a relation is obtained between real strength and n, Fig. 7. The graph shows an increase of f^* for small n and a limiting value of $f^* = f_t$ for $n \to \infty$. Hence n can be conceived as a measure of brittleness. A small value of n makes the material more sensitive to cracks, or, conversely, the apparent strength is small in relation to the real strength of the material. This general conclusion is true of all values of γ. It is obvious that the influence of n is less when the complete softening zone cannot develop (γ small). But even at $\gamma = 0{,}5$ and $n = 0{,}5$ the ratio f^*/f_t becomes 1,35.

Another question concerns the influence of γ on the softening zone size for various values of γ. For instance, could a specimen be too small for the development of complete softening? Fig. 8 can be interpreted as a chart for the qualitative influence of the specimen width on the softening zone size and maximum stress. The wider a specimen, the larger can γ become. On the other hand, in a narrow specimen softening cannot spread so far and therefore γ will stay small, so that the influence on strength is reduced. Fig. 8 has been drawn for $n = 0{,}5$; similar plots can be made for other values of n from Fig. 6.

Up till now the parameters n and γ have been treated without restrictions and without relating them to the behaviour of concrete and the size of a specimen or a struc-

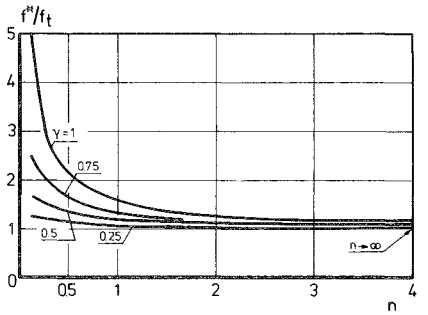

Fig. 7. Real strength to apparent strength in relation to exponent n for various values of γ.

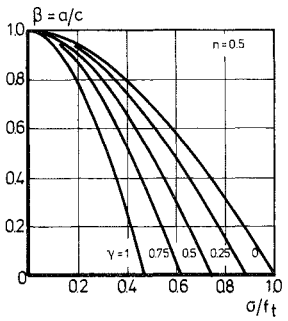

Fig. 8. Size of softening zone vs. remote stress for $n = 0{,}5$ and various γ.

tural member. The parameter n can only be determined in experiments since it depends strongly on the material. The parameter γ is not a geometrical quality, but depends also on n. In the following the relation between n, γ, β and σ/f_t will be considered.

2.2 *Crack tip opening displacement*

Under load, a crack deforms elastically and, in a plastic or softening material, also non-elastically. The crack opens up, which may be visible, or the concrete surrounding the crack stretches plastically. In an elastic-plastic material the two regions can be distinguished by optical measurements. Along the visible part of the crack the stress transfer is zero and along the nonvisible crack, i.e., in the plastic zone, the stress equals the yield strength (three-dimentional effects are neglected here). In concrete micro-cracking develops in the softening zone and the stess releases. The greater the amount of cracking that occurs, the more the deformation will be concentrated at a discrete crack. But even if a crack is visible, stresses are still being transferred across it. Only when the crack opening has reached δ_0 (see Fig. 4), stresses can no longer be transferred. From that point the crack can be called real or stress-free. Although the term "visible" may sometimes be misleading, since micro-cracking can also be observed, it will be used as a synonymon for "stress-free".

The parameter γ depends on the opening displacement of the tip of the visible crack and on the stress deformation curve of concrete as determined in a uniaxial tensile test. If the crack opening has a certain value δ_a the value of γ is given by $(1 - \sigma_t/f_t)$, where σ_t follows from Fig. 4 for $\delta = \delta_a$. In general

$$\gamma = 1 - g(\delta_a/\delta_0) \tag{9}$$

where g is the stress-crack opening function. In order to determine δ_a the crack deformation has to be analysed. The solution given by Ståhle [6] will be used for the purpose and further evaluated.

Ståhle analysed the deformation of a crack in an infinite plate under uniaxial remote normal stress by means of Muskhelishvili's complex potentials [7] and derived the expression for the crack opening displacement as a function of the coordinate x and the

stress distribution function within the plastic region. To give the analysis greater clarity all length terms will be given in dimensionless form.

The general expression then reads for plane stress

$$\alpha\delta(\xi) = -\frac{1}{\beta}\int_{\beta}^{1}\frac{p(t)}{f_t}\left[\ln\frac{(1-\xi^2)^{1/2}+(1-\tau^2)^{1/2}}{|(1-\xi^2)^{1/2}-(1-\tau^2)^{1/2}|}-2\frac{(1-\xi^2)^{1/2}}{(1-\tau^2)^{1/2}}\right]\mathrm{d}t \qquad (10)$$

with

$$\alpha=\frac{\pi E}{2f_t a},\qquad \beta=\frac{a}{c},\qquad \xi=\frac{x}{c},\qquad \tau=\frac{t}{c}$$

Inserting eq. (5) into eq. (10) the expression becomes

$$\alpha\delta(\xi) = -\frac{1}{\beta}\int_{\beta}^{1}\left[1-\gamma\left(\frac{1-\tau}{1-\beta}\right)^n\right]\left[\ln\frac{(1-\xi^2)^{1/2}+(1-\tau^2)^{1/2}}{|(1-\xi^2)^{1/2}-(1-\tau^2)^{1/2}|}-2\frac{(1-\xi^2)^{1/2}}{(1-\tau^2)^{1/2}}\right]\mathrm{d}t \qquad (11)$$

This integral can be solved analytically only for some special values of n. Otherwise it should be treated numerically, but also with caution since there are a few singularities. Finally it turned out that the most successful approach was to split up the whole expression by multiplication into four terms and to solve as much as possible analytically. Then the remainder could solved numerically without problems. Appendix 1 contains a few solutions.

Eq. (11) is an implicit expression for γ, since $\delta_{\xi\to\beta}=\delta_a$ which determines γ with eq. (9). Or in another way, eq. (11) can be solved for various γ and β and the solution is valid for a fixed value of a which is a part of the factor α. To clear up this interrelationship two diagrams are given in Fig. 9, where the dimensionless quantity $\alpha\delta_a$ is plotted against β for $n=0{,}5$ and 2 respectively. It can be seen that the crack tip opening displacement increases with decreasing β. This should be so since a small β means a large softening zone and therefore more deformation. This is true for all values of γ, but the increase is larger for larger γ. Also this is acceptable because $\gamma=1$ stands for complete softening. It is interesting to note that the difference between $\gamma=0{,}125$ and $\gamma=1$ is rather limited. It is larger for $n=2$ than it is for $n=0{,}5$. Also the difference between the

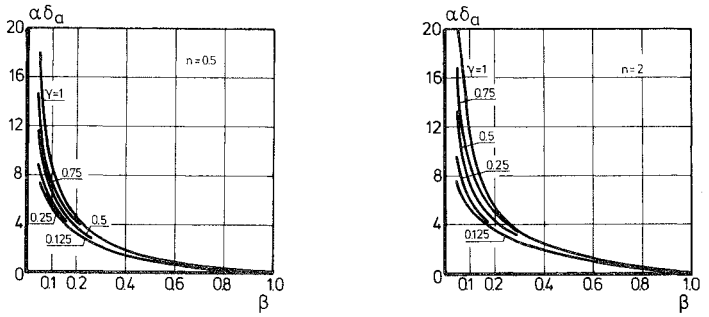

Fig. 9. Crack tip opening displacement as a function of softening zone size and various γ for
a. $n=0{,}5$
b. $n=2$.

two graphs, i.e., between $n = 0{,}5$ and 2, is relatively small compared with the distinct influence on softening zone size (Fig. 6) and strength (Fig. 7). One should not forget, however, that a certain remote stress σ causes a certain β which is smaller with increasing stress. During a tensile test, for instance, Fig. 9 is followed from right to left, while γ is not constant. Since the matter is rather complex, comparisons should only be made for real examples.

The relations can, for example, be used so to determine the dimensions of the specimen that a stress-free crack tip can develop ($\delta_a = \delta_0$). Consider a certain concrete for which E and f_t are known. If no experimental results are available, n has to be estimated, say $n = 0{,}5$. From Fig. 9 $\mathrm{I} = \alpha\delta_a$ can be read as a function of β. From

$$a = \frac{\pi E \delta_0}{2 f_t \cdot \mathrm{I}(\beta)} \tag{12}$$

β can be estimated as follows. If $2a$ is the width of an original crack in a plate of width b, the softening zone c can at most become $b/2$. With $\beta = a/c$ this leads to $a = \beta b/2$ and

$$b = \frac{\pi E \delta_0}{\beta f_t \mathrm{I}(\beta)} \tag{13}$$

Appendix 2 gives an example which shows that the solution for b is not unique but has a certain range depending on β which in turn determines the original crack length $2a$. For larger β, b is larger, but also a is larger. This should be compared with Fig. 6, which shows the connection with the remote stress. So it depends on the aim of the experiment whether a wide or a narrow specimen should be used. Of course, this estimate can only be an approximation, as the relations are derived for a slit in an infinite plate and not for a plate of finite width. Anyhow, it gives an idea of the size required for the proper testing of concrete for softening fracture mechanics.

On the other hand, a certain specimen size may have been used in a tensile test. The question is: what is the probable γ to occur and what is the influence on the tensile strength of the specimen? To answer this question Fig. 9 and Fig. 8 are used together with Fig. 4. Actually, Fig. 4 should be expressed in analytical form. A suitable function may be

$$\frac{\sigma_t}{f_t} = 1 - \left(\frac{\delta}{\delta_0}\right)^k \tag{14}$$

This leads to an expression for γ:

$$\gamma = \left(\frac{\delta_a}{\delta_0}\right)^k \tag{15}$$

Assume a specimen with central crack $2a$ and width b. This leads to a minimum $\beta = 2a/b$. With this β we can read $\mathrm{I} = \alpha\delta_a$ in Fig. 9.

With $\delta_a = \delta_0 \gamma^{1/k}$ and $\alpha = \pi E/(2 f_t a)$ it follows

$$\gamma = \left(\frac{2\mathrm{I} f_t a}{\delta_0 \pi E}\right)^k \tag{16}$$

Since γ was not yet known when reading I from Fig. 9, this procedure is an iterative one. Appendix 3 shows an application of it.

With the aid of these mathematical tools which have been discussed so far, it is possible to predict the crack opening of a tensile specimen as a function of load and the strength as a function of specimen size and initial crack size. The results of the prediction depend on the correctness of the input parameters.

Among these parameters, Young's modulus E, the tensile stength f_t and the stress-free crack opening δ_0 can be determined in uniaxial tests on narrow specimens, whereas the exponent n can be determined from wide precracked specimens.

2.3 *Experimental approach*

Experiments should provide data on the stress crack opening relation eq. (14) and on the exponent n in eq. (4). For the first purpose tensile tests are carried out and for the second the deformation distribution between two saw cuts in a tensile specimen is studied. If the deformation of the softening zone perpendicular to the axis of the crack is described by

$$\frac{\delta(t)}{\delta_0} = \frac{\delta_a}{\delta_0}\left(\frac{c-t}{c-a}\right)^l = \gamma^{1/k}\left(\frac{c-t}{c-a}\right)^l \tag{17}$$

and if the stress crack opening relation conforms to eq. (14), the exponent n becomes

$$n = k \cdot l \tag{18}$$

Results from the literature indicate that k assumes values between 0,2 and 0,4 [8] and l between 1,5 and 2 [9, 10, 11]. This would make n between 0,3 and 0,8. These figures are only rough indications. For a more accurate treatment of plain concrete it was essential to carry out our own experiments. However, fibre-reinforced concrete has recently been treated in a similar way [12].

3 Experiments

3.1 *Experimental programme*

The experimental programme has several aims: first, to provide the input for the analytical model, especially the softening behaviour and the exponent k, second, to provide the data for the deformation distribution around the crack tip, i.e., the exponent l, and third, to supply more information on the cyclic uniaxial behaviour of concrete, particularly in so far as the influence on the softening branch of the stress-deformation and the extension of the softening zone in front of a crack are concerned. The first question was studied by uniaxial deformation-controlled tensile tests on narrow specimens with a rectangular cross-section where E, f_t, δ_0 and the whole stress-deformation curve was determined. The second aim was realized on wide specimens containing two edge slits, also tests in deformation-controlled tensile tests. Finally, the third aim was accom-

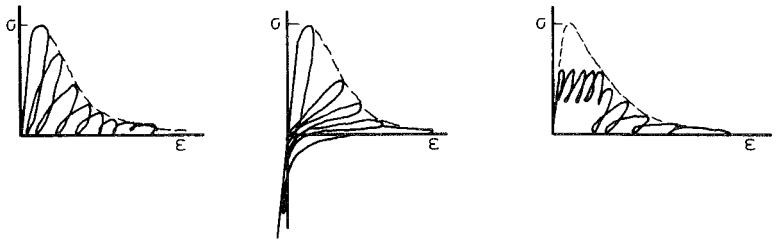

Fig. 10. Types of loading in the experimental programme.

plished with three types of tests (see Fig. 10), namely, cyclic tests up to the envelope curve with a low tensile stress or a compressive stress, respectively, and cyclic tests with a certain number of loading cycles before the top of the stress-deformation curve and subsequent cycling up to the envelope curve. This last-mentioned loading type resembles high-intensity low-cycle fatigue.

All the tests were performed under constant temperature and humidity conditions with a small range of deformation rate. One type of gravel concrete was used with the same curing procedure in all cases. In all, 33 tensile tests were carried out.

3.2 *Experimental method*

3.2.1 Specimens

In order to avoid the wall effect as much as possible the specimens were cut from 50 mm thick panels which were cast in the vertical position. The dimensions of the small specimens were 250 mm long, 60 mm wide and 50 mm thick. A saw-cut of 5 mm × 5 mm on both sides reduced the effective cross-section to 50×50 mm^2. This reduction appeared to be sufficient to initiate fracture in this area. This size of the specimen was a compromise between two requirements: the deformation distribution should be equal over the cross-section, which means that the softening zone should spread uniformly over the whole width, and the cross-section should represent an average concrete. The first requirement would lead to a small specimen whereas the second demands a large one. For a maximum aggregate grain size of 8 mm the present dimensions seemed to be sufficient, which was confirmed by measurements.

Specimens 220 mm in width and 240 mm in length were used for studying the softening zone. Saw-cuts of 5 mm × 20 mm in both edges determined the fracture starting points. The crack should propagate from these points to the centre of the plate and therefore show a continuous transition from elastic to softening deformation.

The preparation of the specimens was as follows: always five panels were cast in a battery mould at the same time. After 3 days the mould was stripped and the panels were stored under water at 20 °C. After a further 11 days the panels were cut to the desired dimensions in such a way that the direction of casting coincided with the direction of testing. The edge saw cuts were made on the same day. The specimens dried in

the laboratory at 20 °C and about 60% relative humidity up to the time of testing (at an age of about 55 days).

Before testing, the upper and lower faces of the specimens were impregnated with a polyester resin in order to improve the strength and adhesion of the glue with which they were mounted in the testing equipment.

3.2.2 Loading equipment

Tests were carried out on a closed-loop electro-hydraulic loading installation which has been used for static and fatigue loading of concrete in recent years [13]. It consists of a 100 kN actuator for alternating tensile and compressive loading, a load cell and the appropriate electronic control unit. It can operate under force or displacement control. In this study two LVDTs (linear variable differential transformers) were mounted on the specimen for monitoring the relative displacement over the crack. The signal was compared with a predetermined one, whereafter the force was adjusted. So a constant rate of deformation of 0,08 and 0,16 μm/s, respectively, was archieved over the whole force range of a static test, i.e., along the complete envelope curve.

In a cyclic test up to the envelope curve the first loading was the same as above. As soon as the force dropped by a certain amount (about 120 N) the control unit switched from the foreward to the reverse movement with the same rate of deformation until a preset force level was reached. This level could be tensile or compressive. At this point

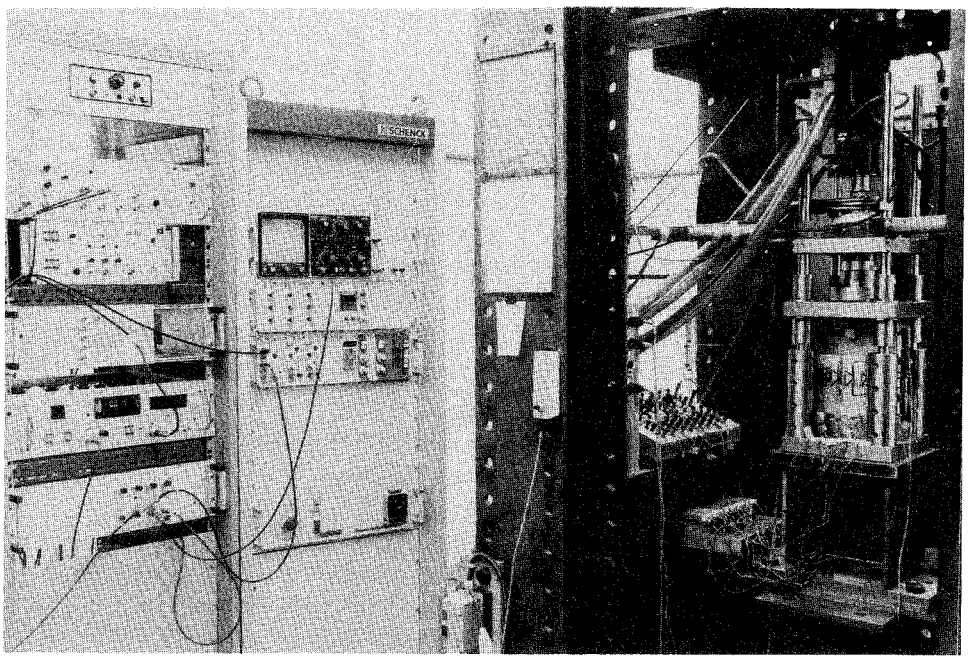

Fig. 11. Testing equipment with guiding device and data acquisition.

the movement was changed again into the foreward direction. These cycles continued up to a maximum relative displacement of 250 μm, at which most of the specimens had already failed.

During the low cycle fatigue tests the first cycles were performed with constant upper and lower stress and constant rate of deformation. After the envelope curve was reached the cycle procedure followed the second control type indicated above.

The specimen was glued between steel platens. The lower platen was fixed to the loading frame whereas the upper was connected to the load cell and subsequently to the actuator, which in turn was connected to the frame via a swivel head. If every part is properly aligned the load acts centrally on the specimen. But due to inhomogeneities in the concrete the stresses and strains may be eccentric. The effect of eccentricity is increased as soon as a crack appears, for the chance that the cracks start and propagate symmetrically is rather small. In the light of these considerations a guiding device was constructed consisting of four stiff rods connected to the base plate and fitting very accurately into roller-bearings. The roller-bearings were connected to the upper loading plate. Calibrating measurements showed that the rotation of the upper plate was not completely prevented but only to such an extent that cracking could always occur from both sides of the specimen simultaneously. Frictional forces in the guiding device were negligible.

Fig. 11 shows the testing equipment. On the left are the electronic control units, on the right the loading frame with specimen, guiding device, load cell and actuator. The equipment was placed in a closed room so that temperature and humidity were almost constant during the test.

3.2.3 Measuring and data acquisition

Deformation measurements were taken by three types of devices: strain gauges, electro-mechanical extensometers and LVDTs. The latter were applied to the sides of the specimens for control purposes. Five extensometers with a gauge length of 35 mm between the tips of the saw cuts were mounted on the front and the rear face of the narrow specimens. In case of wide specimens six 20 mm strain gauges were glued to the front face and two to the rear face. Four extensometers with 35 mm gauge length were additionally applied to both faces. Since the extensometers have a broader measuring range they continue measuring when the strain gauges have already failed.

The measurements were taken with a frequency of 6 Hz and recorded on punched tape. During the test a force-deformation (from LVDT) graph was plotted continuously. The results were later processed in an HP MX21 laboratory computer.

3.3 *Concrete mix and properties*

One medium-strength concrete was used in all the experiments. The mix and the 28-day standard properties are listed in Table 1. Compressive and splitting strength were determined on 33 specimens.

Table 1. Mix and 28-day properties of the concrete

cement:	375 kg/m^3 Portland cement type B (medium-rapid hardening)
water:	187,5 kg/m^3 (water-cement ratio = 0,5)
aggregate:	1268 kg/m^3 sand 0/4 quartzitic material, river gravel 4/8 quartzitic material
cube** compressive strength:	f_c = 47,1 N/mm^2, s^* = 2,83 N/mm^2
tensile splitting strength:	f_{spt} = 3,20 N/mm^2, s = 0,30 N/mm^2

* standard deviation
** 150 mm cubes

3.4 *Results*

3.4.1 Narrow specimens

The results from the narrow specimens are force-elongation curves and, as an example, a deformation distribution over the cross-section of the specimen is represented. The force is divided by the cross-section between the saw cuts, which gives the stress. The elongation of the five extensometers on the front and rear are averaged, which can be expressed as strain until the top of the stress-strain curve is reached. Thereafter the absolute value of the deformation (relative displacement of the two measuring points at 35 mm distance) is an appropriate quantity.

The left-hand diagram in Fig. 12 shows an example of the stress-deformation curve in static loading, while the right-hand diagram represents the deformation distribution over the cross-section. The numbers indicate corresponding states of the test. From the right-hand diagram it can be seen that, with two exceptions, the strains are almost equal over the width of the specimen. At scan No. 2 there is a delay at the centre point, and scans Nos. 4 and 5 show eccentric deformation distribution. Obviously the deformation at the upper edge started to develop faster than at the lower edge. At scan No. 7 the deformations have become almost equal.

From the deformation distribution in this test it can be concluded that the loading and guiding device operated properly. As far as can be judged from these results the

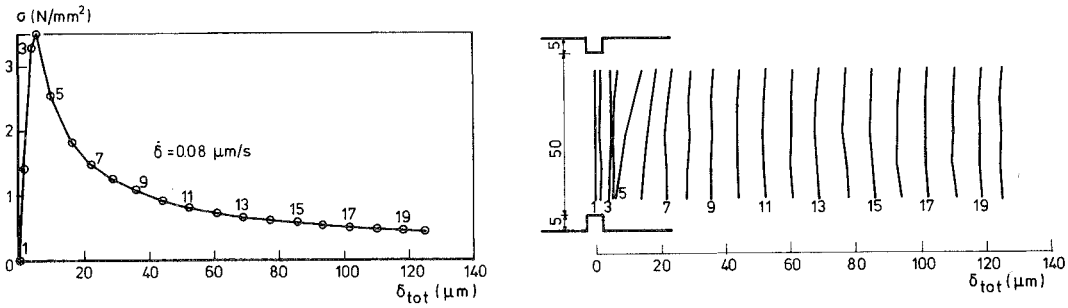

Fig. 12. a. Stress-(average) deformation relation in a static tensile test on a narrow specimen.
b. Deformation distribution over the cross-section. Numbers denote corresponding states during the test.

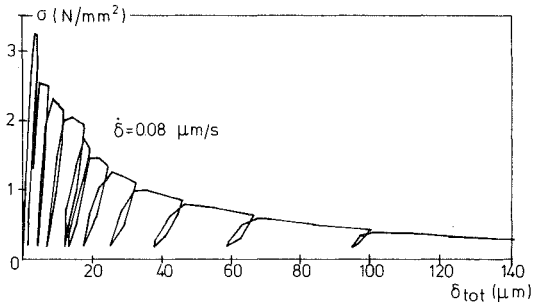

Fig. 13. Stress-deformation relation in a post-peak cyclic test with tensile lower stress.

dimensions of the specimen have been so chosen that a representative stress-deformation curve can be determined.

The left-hand diagram gives the stress vs. average deformation curve. The scans Nos. 0, 1 and 2 lie on a straight line representing the elastic behaviour of concrete. Scan No. 3 is the top of the stress deformation curve, No. 4 is the first post-peak point where the falling-off of the stress is greatest. This is the stage where the deformation distribution of the specimen is eccentric. At the last scan, No. 20, the stress is about one-tenth of the strength. Complete failure occurred at about 250 μm.

An example of a stress-deformation curve for cyclic loading up to the envelope curve is given in Fig. 13, where the lower stress is 5% of the tensile strength. It can be seen that the deformation is not completely reversible. As the total deformation increases, the irreversible part also increases. This feature is also present in Fig. 14, which represents a test in which the lower stress is compressive and amounts to 15% of the tensile strength. The unloading and the loading path of one cycle are quite different, exhibiting a large hysteresis loop.

The loops are still larger when the lower stress is more highly compressive as shown by Fig. 15. Here the lower stress is equal to the average tensile strength.

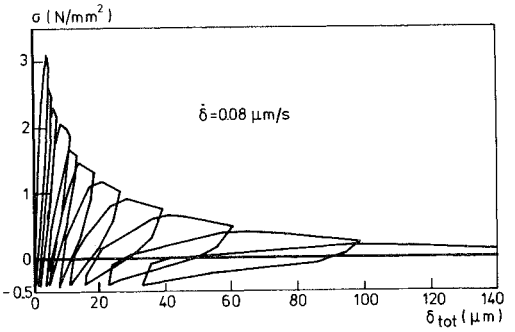

Fig. 14. Stress-deformation relation in a post-peak cyclic test with a small compressive lower stress.

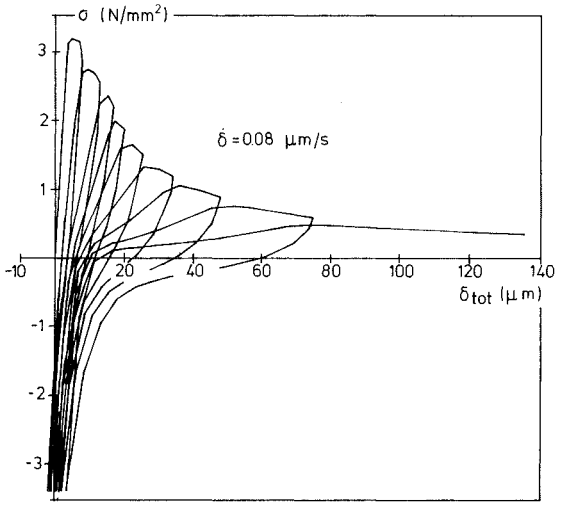

Fig. 15. Stress-deformation relation in a post-peak cyclic test with a large compressive lower stress.

3.4.2 Wide specimens

The purpose of the wide specimens was to create a nonuniform distribution of deformation within the net cross-section. It was expected that the deformation near the tip of the saw-cuts is larger than the average deformation. From the deformation distribution it was possible to estimate the value of l (geometrical exponent). This was done in static experiments.

The same could be done in cyclic experiments with two alternatives: loading until the envelope curve is reached and then cycling to this curve, or cycling in the prepeak range until the envelope curve is reached. A few results of static loading and both types of cyclic loading will be presented.

The left-hand diagram in Fig. 16 shows a stress-average deformation curve obtained from static loading, while the right-hand diagram gives the corresponding deformation distribution. Up to scan No. 5 the deformation distribution is symmetric, exhibiting larger deformation near the saw-cuts than in the middle of the bar. Scans No. 6 to No. 13 are more or less eccentric, indicating a cracking zone starting from the top.

Thereafter the deformation reverts to a uniform distribution. On comparing the actual value of deformation with the deformation at scan No. 15 it can also be seen that long before a limiting deformation is reached (stress free crack opening) the softening zone has spread over the whole cross-section.

Fig. 17 relates to a cyclic test with a lower stress equal to 5% of the tensile strength. This diagram strongly resembles Fig. 13 for the narrow specimen. The deformation distribution is given in Appendix 4. An example where the lower stress is compressive is shown in Fig. 18. Finally, Fig. 19 illustrates a test with an even greater compressive

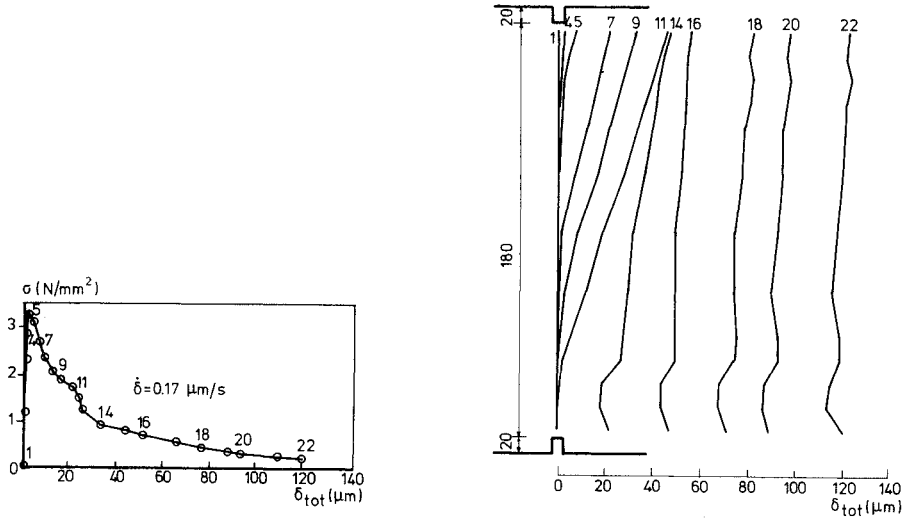

Fig. 16. a. Stress-deformation relation in a static tensile test on a wide specimen.
b. Deformation distribution over the cross-section.

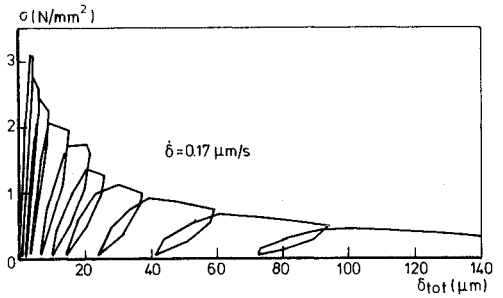

Fig. 17. Cyclic test on a wide specimen with tensile lower stress.

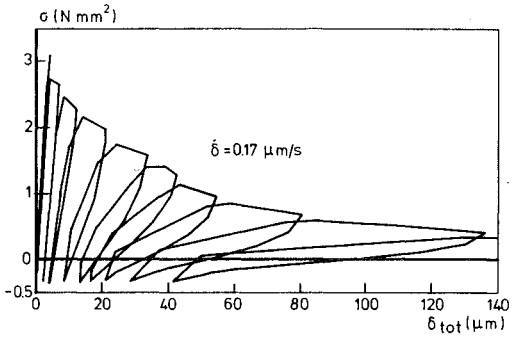

Fig. 18. Cyclic test on a wide specimen with small compressive lower stress.

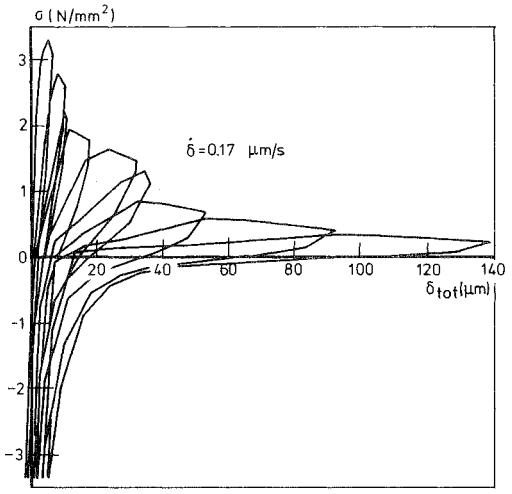

Fig. 19. Cyclic test on a wide specimen with large compressive lower stress.

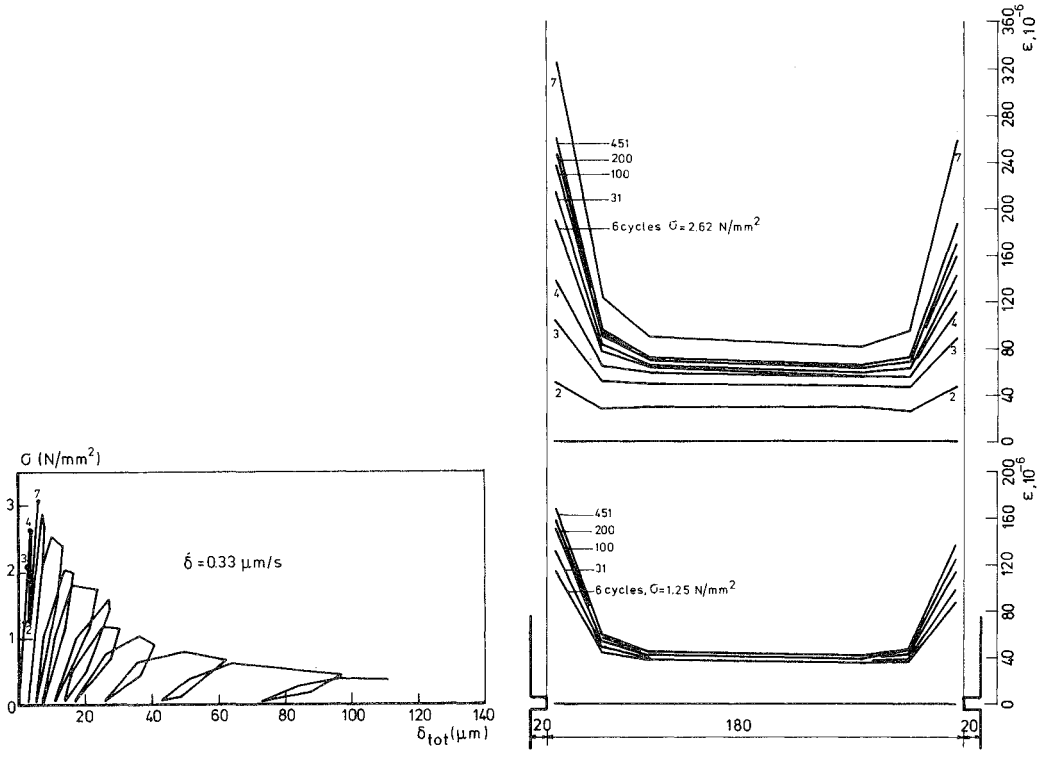

Fig. 20. Prepeak cyclic test on a wide specimen with tensile lower stress.
a. Stress-deformation relation.
b. Strain distribution after various numbers of cycles at upper and lower stress.

stress as the lower stress level. The corresponding deformation distribution is also given in Appendix 4.

The second type of cyclic tests will be illustrated by the following two diagrams. The stress deformation curve in Fig. 20 shows the initial loading to scan No. 4 and subsequent cycling between 25 and 85% of the tensile strength. Because no fracture had occurred after 457 cycles the load was raised to scan No. 7 when the envelope curve was reached. How the deformation developed during cycling is represented in the right-hand part of Fig. 20. Here the strain has been plotted for various numbers of cycles. Strain has been chosen because the top of the stress-strain diagram was not yet reached and no crack was present. It can be seen that the strain is concentrated near the tip of the saw-cut and especially the strain in this part of the specimen grows most rapidly. Between scans Nos. 3 and 4, a value of 100 micro-strain is reached, which becomes almost 200 micro-strain after 451 cycles. Even after unloading to the lower stress level the maximum strain is about 150 micro-strain.

A similar result is exhibited in Fig. 21 for a test with greater compressive stress as the lower stress level. First, the specimen was loaded to 85% of the tensile strength, then 75 cycles were performed between $-f_t$ and $0{,}85\,f_t$, then 39 cycles were performed with a higher stress level, and finally the envelope curve was followed by another 8 cycles. The strain distribution shows how the strains grow during cycling under tensile and com-

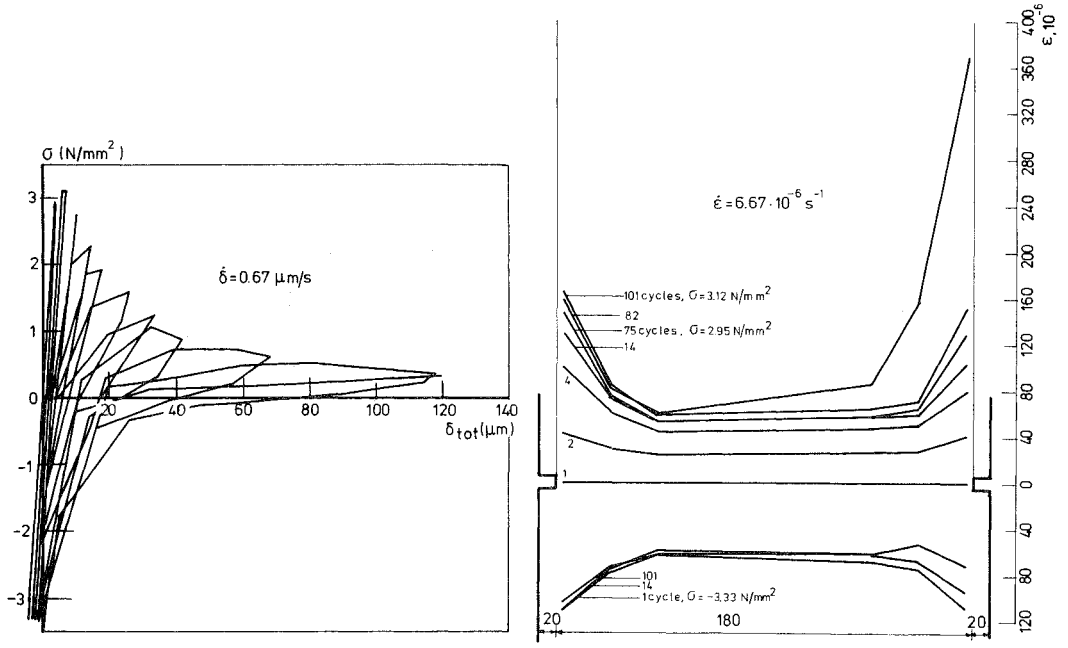

Fig. 21. Prepeak cyclic test on a wide specimen compressive lower stress.
a. Stress-deformation relation.
b. Strain distribution after various numbers of cycles at upper and lower stress.

pressive stress. The strain is again concentrated near the tips of the saw-cuts. Up to 82 cycles the specimen deforms almost symmetrically, but afterwards deformation on the right-hand side proceeds more rapidly. It is interesting to note that the strain under compressive load then decreases with increasing number of cycles.

These results will be discussed in the next paragraph. The static test results will be used for the input and verification of the fracture mechanics model. The cyclic results will be interpreted in a more qualitative way.

4 Discussion of the results of static tests

4.1 *Stress-deformation relation*

By definition, the test results of the narrow specimens will be considered as representative of the material, i.e., it is assumed that there is no crack and that a uniform distribution of deformation exists. Furthermore an elastic softening material model will be applied, which implies a straight stress-strain line up to the tensile strength. Both assumptions are partly true, which is apparent from Fig. 11. On the other hand, it is a rather limited simplification and can be accepted for the purpose of modelling.

The stress-deformation relation comprises four essential quantities: the elastic modulus E, the tensile strength f_t, the stress-free crack opening δ_0 and the exponent k in eq. (14). The elastic modulus is determined from the readings of two long extensometers (100 mm), which were mounted in the middle of the faces of the specimen, and from the applied stress equal to $0{,}6 f_t$. The average value was 39 250 N/mm^2. The average tensile strength was 3,2 N/mm^2. All the results (also of the cyclic tests) have been used for the averaging.

When the elastic modulus was known, the total deformation could be split into two parts: the elastic part which is $\delta_{el} = \sigma \cdot l_{meas}/E$ (where l_{meas} is the gauge length equal to 35 mm) and the remaining part which is called the crack opening. The stress vs. crack opening relation was fitted by the least square method and the power function of eq. (14). The best fit for all the results was obtained with $k = 0{,}31$ and $\delta_0 = 0{,}175$ mm. The range of k extended from 0,29 to 0,40, and δ_0 could assume values between 0,120 and 0,200 mm for the individual specimens. It should be noted that the results of the cyclic tests on narrow specimens have been used as well, since there were no significant differences between the envelope curves for static and for cyclic tests, respectively. Two examples of $\sigma - \delta$ curves are presented in Appendix 5.

With these results the fracture energy G_f can be determined according to

$$G_f = \int_0^{\delta_0} \sigma(\delta)\, \mathrm{d}\delta \tag{18}$$

With eq. (14) it follows that

$$G_f = f_t \delta_0 \frac{k}{k+1} = 132{,}5 \text{ N/m} \tag{19}$$

The mean value for all the narrow specimens was calculated as 135 N/m, which agrees closely with the value above. Similar values have been reported from several investigations [19].

4.2 *Deformation of the softening zone*

The specimens were too small for the creation of a completely developed softening zone. There was always stress at the tip of the saw-cut and no crack-free crack mouth could be obtained. This can readily be seen from Fig. 16, which gives the deformations and can be compared with Fig. 4. This means that the factor γ of eq. (5) is smaller than one.

First the exponent l should be determined from strain measurements on a wide specimen. Therefore the small deformations of the specimen will be examined on which Fig. 16 was also based. Fig. 22 shows subsequent steps of the total deformations drawn to a larger scale than in Fig. 16. If the elastic part is subtracted from the total deformation, the deformation of the softening branch is obtained. With the tensile strength of 4,20 N/mm^2 and an elastic modulus of 50 750 N/mm^2 for a narrow companion specimen (the age at testing was 102 days in this specific case) the elastic strain becomes $\varepsilon = 4{,}2/50750 = 83$ micro-strain. Since the gauge length is 35 mm, the elastic deformation is

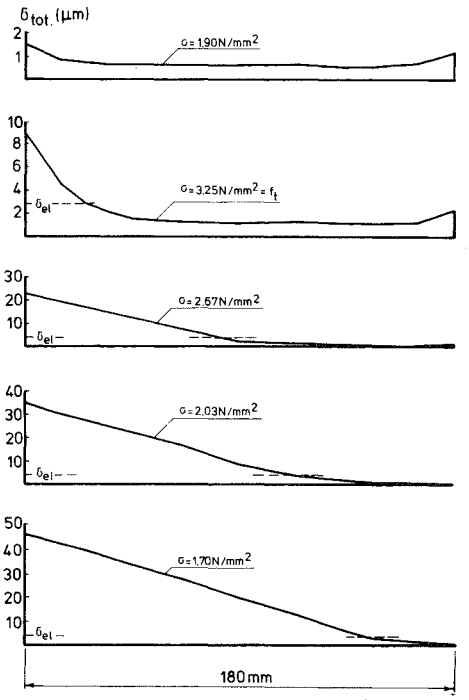

Fig. 22. Deformation distribution of a wide specimen in a static test (elastic limit: 2,9 μm).

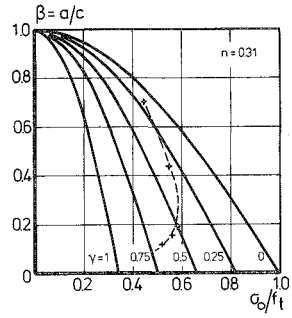

Fig. 23. Softening zone size vs. remote stress for $n = 0{,}31$ and various values of γ. The dotted line represents subsequent loading states of a wide specimen.

$\delta_{el} = 2{,}9 \cdot 10^{-3}$ mm. Taking this value as a reference line it turns out that the deformation of the softening zone is a straight line with a slope of 0,017 deg. This means $l = 1$ and $n = 0{,}31$.

For various loading steps γ can be calculated from $\gamma = (\delta_a/\delta_0)^{0{,}31}$, where δ_a is the measured deformation at the tip of the saw-cut. At the same time the size of the softening zone can be determined from Fig. 22 and therefore β is known. The appropriate values of γ and β are given in the diagram. With these values the measured ratio σ_0/f_t can be checked with the aid of Fig. 23. The dotted line connects five loading steps. The loading starts with a small value of γ and a large value of β. With higher loading γ increases, whereas β decreases. At some point a maximum load is reached, which should correspond to the farthest right-hand point of the dotted line. In this particular case it is 0,59 f_t. This value should be compared with the experimentally determined value of 3,25 N/mm^2 referred to $f_t = 4{,}20$ N/mm^2; hence $\sigma_0/f_t = 0{,}77$. There are several reasons for this divergence: first, it has already been mentioned that the model has been derived for a centre crack, whereas the specimen has side cracks. The maximume influence of this error is estimated at 5%. Secondly, the specimen is not loaded in purely concentric manner. Since β is calculated from the left-hand softening zone, the influence of softening is overestimated in relation to an average influence. Thirdly (and this is likely to cause a considerable deviation), the stress-deformation curve has been measured on specimens also with saw-cuts, which means that f_t cannot be the "real" strength of the material. Therefore the reference value is too low.

It is not proposed to work out these influences in more detail. For that purpose more tests would have to be performed on two sets of specimen geometry which are further apart than has been envisaged in this investigation. On the other hand, Fig. 23 shows how to use the model and how to interpret tensile tests on an elastic softening material.

5 Discussion of the results of cyclic loading

5.1 *Stiffness degradation*

The modelling of the cyclic behaviour is still in course of development, and for this

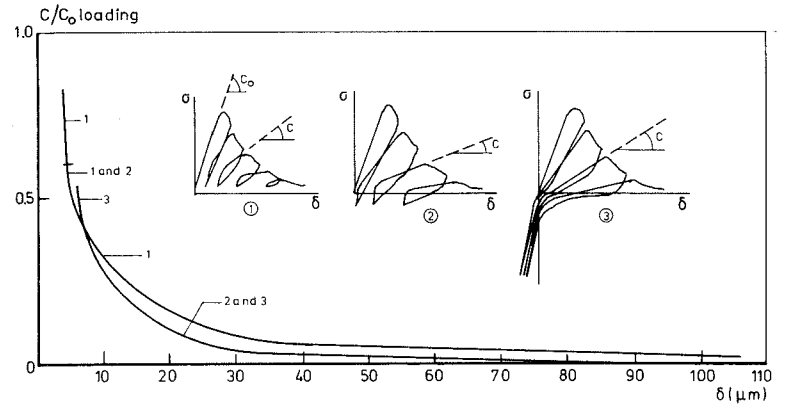

Fig. 24. Degradation of stiffness during cyclic loading, loading path.

reason the picture is not yet as clear as for static loading. Here only a few characteristics will be discussed, which follow immediately from Figs. 13 to 15. These show that the stiffness of the specimen decreases with each loading cycle. If the relative stiffness C/C_0 is, in Fig. 24, plotted versus the total deformation which has been reached on the envelope curve, a very steep decline in stiffness can be seen. Already at a total deformation of 10 μm the stiffness is only 30% of its original value. The type of loading is of less importance. The stiffness of the unloading path appears to be greater than of the loading path. A similar diagram is shown for this case (Fig. 25).

This behaviour can be interpreted as follows. It is assumed that the whole cross-section has reached the softening stage, which means that there are micro-cracks which can open and close. If the material were elastic no irreversible strain would occur. Obviously it is not, indicating that frictional processes play a part. On the other hand, the reversible deformation is rather large even when the remaining stress at the envelope curve is already small. An illustration of such a material consisting of cracks

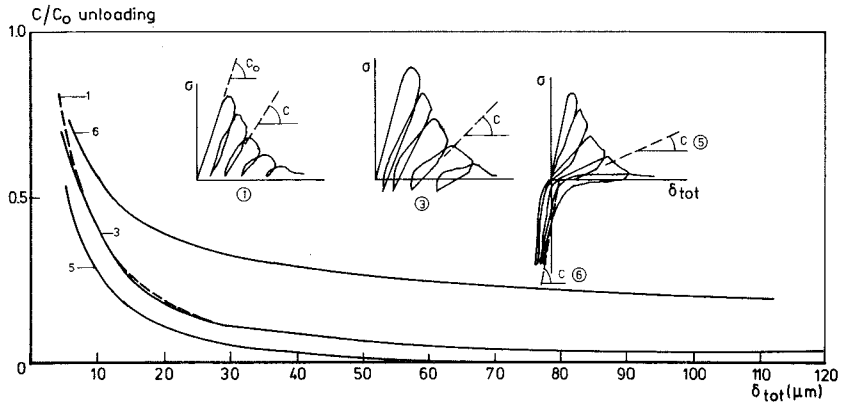

Fig. 25. Degradation of stiffness during cyclic loading, unloading path.

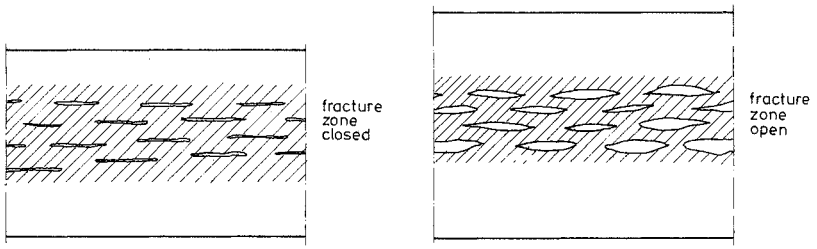

Fig. 26. Schematic representation of microcracked zone
a. unloaded
b. loaded.

and undamaged material is given in Fig. 26. The left-hand part shows the unloaded, and the right-hand part the loaded stage.

Various stages can be distinguished in a cyclic stress-deformation curve: elastic elongation of the specimen, small crack opening, elastic unloading, crack closing. From the slope of the lines it can be said that in each cycle the cracked zone increases and that the crack faces no longer match. Some regions will be stressed in compression even if the remote average stress is tensile. When the average lower stress is compressive, the crack faces are forced together, which is confirmed by stiff, rather elastic behaviour on reloading.

In regard to the large absolute displacement as recorded in the alternating stress cycles, a cracking zone should be assumed which consists of voids which are interconnected by bridges as shown in Fig. 26. These bridges undergo bending which leads to higher deformation than normal force would cause. This is a rather qualitative description which is helpful in understanding the phenomena. For quantitative use the stress-deformation curves should be taken as a basis and described by a mathematical formula. This would enable them to be used in a finite element computer programme [20].

5.2 *Extending softening zone*

Contrary to the tests with cyclic loading up to the envelope curve, the specimens in the tests with prepeak cyclic loading do not have a softening zone over the whole cross-section. They start with a small softening zone around the saw-cuts and only later reach the envelope curve. For this intermediate state of progressive damage another model is presented in Fig. 27. Assume a crack in front of which a certain softening zone has developed (Fig. 27a). After N cycles the crack length $a(N)$ and the softening zone have extended to $c(N)$. During unloading, elastic strains recover but, because in the softening zone the material has been deformed beyond the elastic limit, it will not recover completely. The parts which are strained too much, i.e., at the real crack tip, will have to be compressed in order to follow the unloading deformation. After complete release of the external stress there will remain self-equilibrating residual stresses (Fig. 27b). The

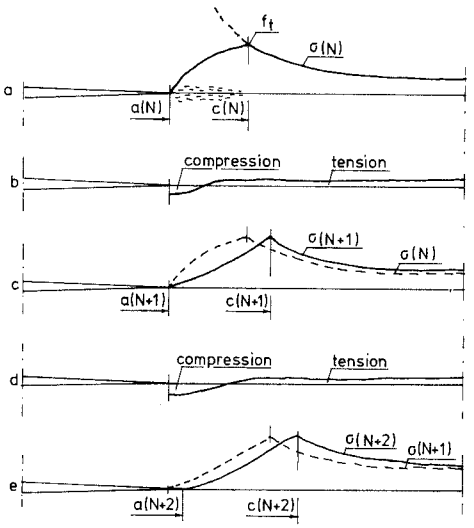

Fig. 27. Crack growth in an elastic softening material during cyclic loading.

distribution of these stresses depends on the stress-deformation relation of the material. For ideal elastic-plastic material they can be calculated [21]. There is no doubt that the loading history of all the points in the softening zone is different in regard to upper and lower stress and stress range during one cycle.

During the second loading cycle the stress distribution according to Fig. 27a would be obtained only if the material in the softening zone were not affected by unloading. This seems unrealistic, sonce concrete shows irreversible strains under uniaxial loading, which means, for instance, that a point in the softening zone with a certain irreversible strain (or deformation) follows the same deformation as in the first cycle but finally attains a larger deformation (approximately the sum of irreversible plus loading deformation). Because this point has already reached the descending part of the stress-strain relation, it now follows that the line and consequently the stress is lower than in the first loading. The new stress distribution may be as shown in Fig. 27c, where the softening zone has spread a little in order to ensure total equilibrium.

In a following cycle the same procedure is repeated. The softening zone will extend farther. Whether the real crack length a will also increase depends upon the development of the deformation (Fig. 27e). By definition, the real crack starts when $\delta = \delta_0$, and therefore it depends on the crack shape during cycling whether the crack proceeds or not.

According to this mechanism the total elongation of a tensile specimen under maximum stress increases gradually during cycling because the elastic stress in the area adjacent to the softening zone increases, which causes elastic strain. The irreversible deformation in the softening zone may also increase, causing higher residual stresses, both compressive and tensile. The tensile stress amplitude will therefore decrease,

thereby simulating a stiffer overall response of the specimen. Deterioration of the crack faces may occur and may change the situation. However, the softening zone continues to spread until no part of the cross-section is able to resist tensile stress. Then failure will occur.

Whether a quantitative treatment of the cyclic behaviour is possible depends on whether the stress-strain relation as a function of the number of cycles and lower stress is known and on the shape of the crack during cycling. If the knowledge were available, not only constant-amplitude loading but also block loading could be treated.

For the present, it will only be qualitatively checked whether there is evidence of such a behaviour.

For this reason the deformation has been measured during cycling on wide specimens. A few scans will be sketched to demonstrate the deformation behaviour. The test started with an upper stress of 2,63 N/mm^2 and a lower stress of 1,27 N/mm^2; later the upper stress was increased to 2,95, and finally to 3,12 N/mm^2 in order to provoke failure. Fig. 21 gives the strains over the width of the specimen at the first loading (scans Nos. 1, 2, 4) and after a number of cycles as indicated in the diagram. First the strains are smaller than the elastic strains (in this example: $f_t = 4{,}20$ N/mm^2, $E = 47800$ N/mm^2, $E_{el} = 88$ μstrain). At scan No. 4 the edge strain already exceeds the elastic limit, and so a softening zone starts to develop. At higher loading this zone expands, as is apparent on comparing the distribution after 14 and 75 cycles respectively. The same appears between 82 and 101 cycles at a higher stress. During the same time the irreversible strain at lower stress increases.

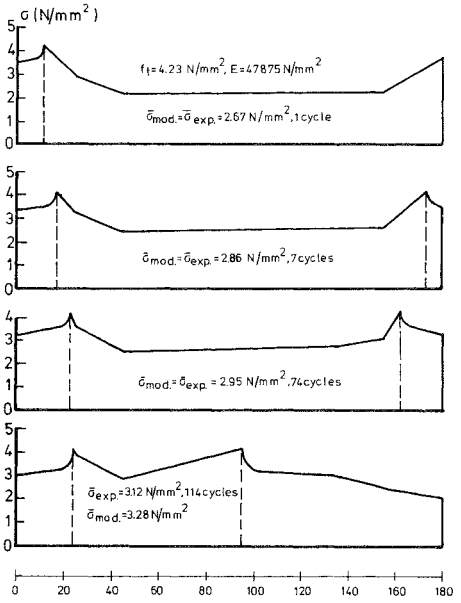

Fig. 28. Stress distribution in a wide specimen during cyclic loading (corresponds to Fig. 21).

Since the stress-deformation curve is known from narrow companion specimens the stress distribution can be calculated. A few selected stages are given in Fig. 28 (for others see Appendix 6). The topmost three lines show how the stress peak (tensile strength) moves inwards during cycling without stress increase. The lower lines correspond to a higher stress. It can also be seen that the softening zone spreads during cyclic loading. In this case the governing crack develops from the right hand side. After 114 cycles the envelope curve was reached and the remote stress decreased.

The total force has been calculated by integrating the area under the stress distribution curve. The force has been divided by the cross-sectional area, giving an average stress designated by $\bar{\sigma}_{\text{model}}$. During the experiment the remote stress $\bar{\sigma}_{\text{exp}}$ was applied. It can be seen that the two stress values are equal in the beginning, but later tend to deviate a little. However, the difference remains small.

It can be concluded that this experiment produced the behaviour which had been expected from the qualitative model of Fig. 27. It is desirable to carry out further studies to elaborate this idea which produces appropriate results for elastic yielding material [22] but has never been applied to softening material so far as the author is aware.

6 Conclusions

Concrete is modelled as a linear elastic softening material and introduced into fracture mechanics. The stresses in the softening zone of a discrete crack are assumed to conform to a power function. The exponent n of this function can be split up into a mechanical part and into a geometrical part if the initial stress-deformation curve and the crack geometry are also described by power functions. It has been shown that the exponent n has an essential effect on the loadbearing capacity of a cracked plate. The smaller the value of n, lower is this capacity in relation to the tensile strength of the material. Though not treated in this investigation, it can be assumed that the power n decreases with higher concrete quality. Thus, high-strength concrete would be more sensitive to cracks than low strength concrete according to this model.

By working out the crack opening-displacement relation the effect of the size of a plate (or specimen) on the softening zone and the loadbearing capacity of a plate was shown. It is demonstrated that large specimens are required if a complete softening zone is to be studied or, on the other hand, that ordinary specimens are only slightly affected by non-uniform stress distribution.

These theoretical findings are verified by experiments on a medium-strength concrete. In uniaxial deformation-controlled tensile tests on narrow specimens the complete stress-deformation curve was established. Furthermore the effect of repeated tensile and alternating tensile compressive stresses on the envelope curve was studied. No significant effect was detected. It proved possible to describe the stress-deformation curve with sufficient accuracy by a simple power function. The deformation distribution over the cross-section was measured on wide specimens. It turned out that the deformation is linearly distributed in the softening zone; so the geometrical power function is just a linear function. With the aid of the two functions the loadbearing capacity

was compared with the experimentally obtained value. Having regard to the approximations made, there was reasonably good agreement.

During cyclic tests the stiffness degradation and the increase of irreversible deformation was studied. It is stated that the softening zone consists of micro-cracks within an undamaged material. This zone can be modelled by voids and elastic bridges which are bent by an external load. The subsequent stages during post-peak cyclic loading can be represented, such as elastic crack opening, crack extension, crack closure and – in compressive loading – forced closure of cracks.

On the other hand, prepeak cyclic loading can be explained by the extension of softening zones. This behaviour has been illustrated by a simple physical model. The features of this model emerged from strain measurement in the vicinity of a crack during cyclic loading.

In conclusion it can be stated that the behaviour of concrete is appropriately modelled by nonlinear fracture mechanics. Since the experiments have been performed on one concrete mix only, it is proposed to verify this statement also on concrete of different composition and quality. Cyclic loading which has a detrimental effect on concrete in the prepeak and the post-peak range can also be modelled by fracture mechanics. For the time being, only qualitative models for cyclic behaviour have been presented. Having regard to the experimental results obtained, it is strongly recommended to continue along this line of investigation.

7 Acknowledgements

The author is indebted to Ir. J. M. Moelands who carried out his graduation work in this field. He performed the tests on the basis of the theoretical model and carefully analysed them. Furthermore, the assistance of Dr. Ir. H. A. W. Cornelissen and Ing. G. Timmers is gratefully acknowledged.

8 Notation

a half initial crack length
b specimen width
C crack opening sitffness
c half crack length with softening zone included
E Young's modulus
f_t tensile strength
f^* real strength (contrary to apparent strength f_t)
G_f fracture energy
I value of an integral
K_p stress intensity factor due to closing stress p in softening zone
K_σ stress intensity factor due to remote stress σ
k exponent in stress crack opening relation
l exponent in crack geometry relation

n exponent in stress softening zone relation
p closing stress in softening zone
r polar coordinate
t coordinate
x coordinate
α $= \pi E/(2f_t a)$
β $= a/c$
γ coefficient accounting for partial crack opening
δ deformation or (relative) crack opening displacement
δ_a crack tip opening displacement
δ_0 stress free crack opening
δ_{el} elastic deformation
θ polar coordinate
ξ $= x/c$
σ stress
τ $= t/c$

9 References

1. DUGDALE, D. S., Yielding of steel sheets containing slits, J. Mechanics and Physics of Solids 8 (1960), pp. 100–104.
2. BARENBLATT, G. I., The mathematical theory of equilibrium cracks in brittle fracture, Advances in Applied Mechanics 7 (1962), pp. 55–129.
3. THEOCARIS, P. S. and E. E. GDOUTOS, The modified Dugdale-Barenblatt model adapted to various fracture configurations in metals, Int. J. of Fracture 10 (1974), No. 4, pp. 549–564.
4. HILLERBORG, A., Analysis of fracture by means of the fictitious crack model, particularly for fibre reinforced concrete, Int. J. of Cement Composites 2 (1980), pp. 177–184.
5. SIH, G. C. ed., Mechanics of fracture. I. Methods of analysis and solutions of crack problems, Noordhoff Int. Publ., Leyden, 1972.
6. STÅHLE, P., On the small crack fracture mechanics,Int. J. of Fracture 22 (1983), pp. 203–216.
7. MUSKHELISHVILI, N. I., Some basic problems of the mathematical theory of elasticity, P. Noordhoff Ltd., Groningen 1953.
8. PETERSSON, P. E., Crack growth and development of fracture zones in plain concrete and similar materials. Report TVBM-1106, Lund, Sweden, 1981.
9. NAUS, D. J., Applicability of linear-elastic fracture mechanics to Portland cement concretes. Cited by Z. P. Bažant and B. H. Oh, RILEM Materials and Structures 16 (1983), No. 93, pp. 155–177.
10. CEDOLIN, L., S. DEI POLI, and I. IORI, Analisi spezimentale de processo di formazione della fratture nel calcestruzzo, Studi e Ricerche Politechnico di Milano, No. 3, 1981.
11. HEILMANN, H. G., Zugspannung und Dehnung in unbewehrten Betonquerschnitten bei exzentrischer Belastung, DAfStb 269, Berlin 1976.
12. VISALVANICH, K. and A. E. NAAMAN, Fracture model for fibre reinforced concrete, ACI Journal 80 (1983), No. 2, pp. 128–138.
13. CORNELISSEN, H. A. W. and G. TIMMERS, Fatigue of plain concrete in uniaxial tension and in alternating tension-companion. Experiments and results, Report No. 5-81-7, Stevin Laboratory, Delft University of Technology, Delft, The Netherlands 1981.
14. IABSE, Intern. Colloquium "Advanced Mechanics of Reinforced Concrete", Delft, 1981.
15. State-of-the-Art Report on Finite element analysis of reinforced concrete, ASCE, New York, 1982.

16. KÖNIG, G. und M. JAHN, Über die verschiedenen Erscheinungsformen der Betonzugfestigkeit und ihre Bedeutung für das Tragverhalten von Massivbauten, Beton- und Stahlbetonbau 78 (1983), No. 9, pp. 243–247, No. 10, pp. 281–286.
17. CEB, Detailing of concrete structures. First draft of a design manual, CEB Bulletin d'information, No. 150, Paris, 1982.
18. TERRIEN, M., Emission acoustique et comportement mécanique post-critique d'un béton sollicité en traction, Bull. Liaison Ponts et Chausées 105 (1980), janv.-févr., pp. 65–72.
19. HILLERBORG, A., Concrete fracture energy tests performed by nine laboratories according to a draft RILEM recommendation, Lund Inst. of Techn. TVBM 3015, Lund, Sweden, 1983.
20. MOELANDS, J. M., Modelmatige omschrijving van het vermoeiingsgedrag van ongewapend beton onder wisselende en herhaalde belasting. Deel 4. Numeriek onderzoek, Graduate thesis, Delft University of Technology, 1984.
21. SCHWALBE, K. H., Bruchmechanik metallischer Werkstoffe, Hanser, München, 1980, pp. 56–72.
22. FÜHRING, H. and T. SEEGER, Dugdale crack closure analysis of fatigue cracks under constant amplitude loading, Eng. Fracture Mechanics 11 (1979), No. 1, pp. 99–122.

APPENDIX 1

Crack tip opening displacement

After multiplication eq. (11) contains four integrals. The first is

$$I_1 = \int_{\beta}^{1} \ln \frac{(1-\xi^2)^{1/2} + (1-\tau^2)^{1/2}}{|(1-\xi^2)^{1/2} - (1-\tau^2)^{1/2}|} \, dt \tag{A1}$$

The solution is

$$I_1 = -\beta \ln \frac{(1-\xi^2)^{1/2} + (1-\beta^2)^{1/2}}{|(1-\xi^2)^{1/2} - (1-\beta^2)^{1/2}|} + 2 \arcsin (1-\beta^2)^{1/2} -$$

$$- \xi \left[\operatorname{arcosh} \frac{1 + (1-\xi^2)^{1/2}(1-\beta^2)^{1/2}}{(1-\xi^2)^{1/2} + (1-\beta^2)^{1/2}} - \operatorname{arcosh} \frac{1 - (1-\xi^2)^{1/2}(1-\beta^2)^{1/2}}{(1-\xi^2)^{1/2} - (1-\beta^2)^{1/2}} \right] \tag{A2}$$

$\xi \to \beta$ is finite.

The second integral is

$$I_2 = -\int_{\beta}^{1} 2 \frac{(1-\xi^2)^{1/2}}{(1-\tau^2)^{1/2}} \, dt = -2(1-\xi^2)^{1/2} \arcsin (1-\beta^2)^{1/2} \tag{A3}$$

The third term becomes

$$I_3 = -\int_{\beta}^{1} \gamma \left(\frac{1-\tau}{1-\beta} \right)^n \ln \frac{(1-\xi^2)^{1/2} + (1-\tau^2)^{1/2}}{|(1-\xi^2)^{1/2} - (1-\tau^2)^{1/2}|} \, dt \tag{A4}$$

which has been solved numerically with Simpson's rule.

The fourth integral is

$$I_4 = \int_{\beta}^{1} 2\gamma \left(\frac{1-\tau}{1-\beta} \right)^n \frac{(1-\xi^2)^{1/2}}{(1-\tau^2)^{1/2}} \, dt \tag{A5}$$

This has been solved analytically for $n = \frac{1}{2}$, 1, 2, 4 respectively, leading to the following expressions:

$$n = \tfrac{1}{2} \qquad I_4 = 4\gamma \frac{(1-\xi^2)^{1/2}}{(1-\beta)^{1/2}} [\sqrt{2} - (1+\beta)^{1/2}]$$

$$n = 1 \qquad I_4 = 2\gamma \frac{(1-\xi^2)^{1/2}}{1-\beta} [\arcsin (1-\beta^2)^{1/2} - (1-\beta^2)^{1/2}] \tag{A7}$$

$$n = 2 \qquad I_4 = 2\gamma \frac{(1-\xi^2)^{1/2}}{(1-\beta)^2} \left[\frac{3}{2} \arcsin (1-\beta^2)^{1/2} - 2(1-\beta^2)^{1/2} + \frac{\beta}{2} (1-\beta^2)^{1/2} \right] \tag{A8}$$

$$n = 4 \qquad I_4 = 2\gamma \frac{(1-\xi^2)^{1/2}}{(1-\beta)^4} \left[\frac{35}{8} \arcsin (1-\beta^2)^{1/2} + (1-\beta^2)^{1/2} \left(-4 + 3\beta + 4 \frac{\beta^2 - 2}{3} + \frac{\beta(2\beta^2+3)}{8} \right) \right] \tag{A9}$$

The cases $n = 1/4$ and $1/8$ can be approximately treated by series expansion, which will affect the accuracy of the results.

APPENDIX 2

Example of specimen size estimation

Eq. (13) gives the relation between specimen width and crack tip opening displacement. For $\pi E\delta_0/f_t = 2200$ mm, $n = 0{,}5$, $\gamma = 1$ Fig. 9a gives

I = 1,8 for $\beta = 0{,}4$, then: $b = 2200/(0{,}4 \cdot 1{,}3) = 3055$ mm and $a = 611$ mm

I = 4,4 for $\beta = 0{,}2$, then: $b = 2200/(0{,}2 \cdot 4{,}4) = 2500$ mm and $a = \frac{b}{2} \cdot \beta = 250$ mm

I = 9,0 for $\beta = 0{,}1$, then: $b = 2200/(0{,}1 \cdot 9{,}0) = 2444$ mm and $a = 122$ mm

If the concrete has a higher tensile strength for equal elastic modulus, for instance, with a higher cement content and a lower water-cement ratio, the specimens could be less wide (for $n = \text{const}$). On the other hand, if the elastic modulus increases due to stiffer aggregate and the tensile strength remains the same, the specimen width should be larger.

APPENDIX 3

Determination of γ for a certain specimen size

Eq. (16) shall be evaluated for $\pi E\delta_0/f_t = 2200$ mm again, k is taken as 0,3, $n = 0{,}5$, $b = 300$ mm and $a = 15$ mm. This gives

$$\beta = \frac{2a}{b} = 0{,}1$$

For $\beta = 0{,}1$ and $\gamma = 0{,}5$ we obtain from Fig. 9a: $I = 6{,}6$.

With the aid of eq. (16) $\gamma = 0{,}49$, which is practically the same as the assumed γ. From Fig. 8 we obtain for $\beta = 0{,}1$, $\gamma = 0{,}5$, $n = 0{,}5$ the stress-strength ratio as 0,70, i.e., the strength of such a specimen would be 0,7 times the uniaxial strength of an uncracked specimen. The deformation δ_a follows from eq. (15); for $\delta_0 = 0{,}175$ mm it is $\delta_a = 0{,}017$ mm

APPENDIX 4

Deformation distribution of wide specimens

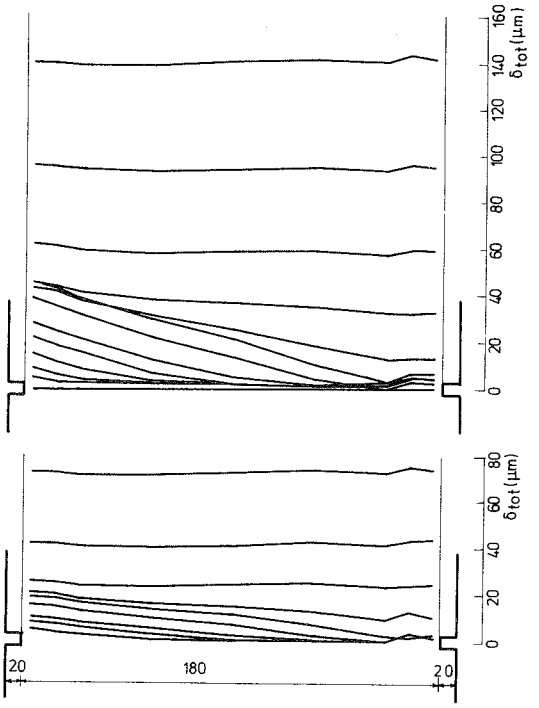

Fig. A4.1 Deformation distribution of specimen of Fig. 17. Upper part: deformation at stresses of envelope curve. Lower part: deformation at lower stress.

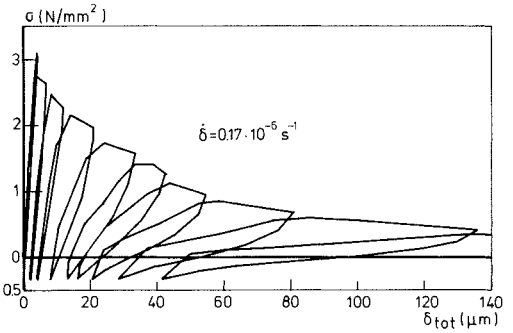

Fig. A4.2 Stress deformation curve of a test with a small compressive lower stress.

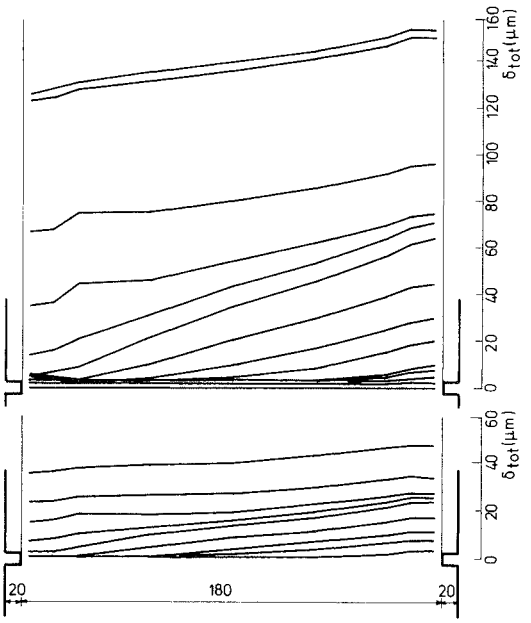

Fig. A4.3 Deformation distribution of the test of Fig. A4.2. Upper part: deformation at envelope stresses. Lower part: deformation at lower stress.

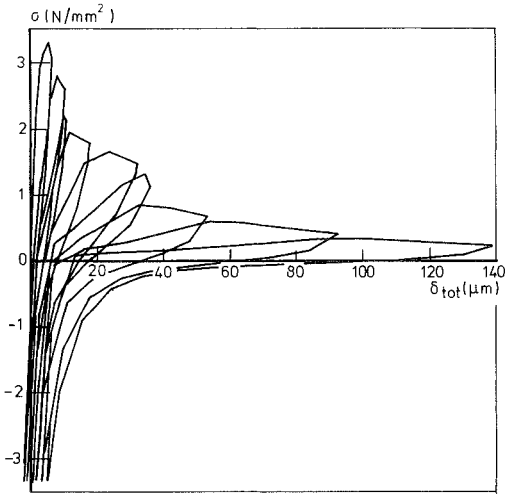

Fig. A4.4 Stress deformation curve of a test with a high compressive lower stress.

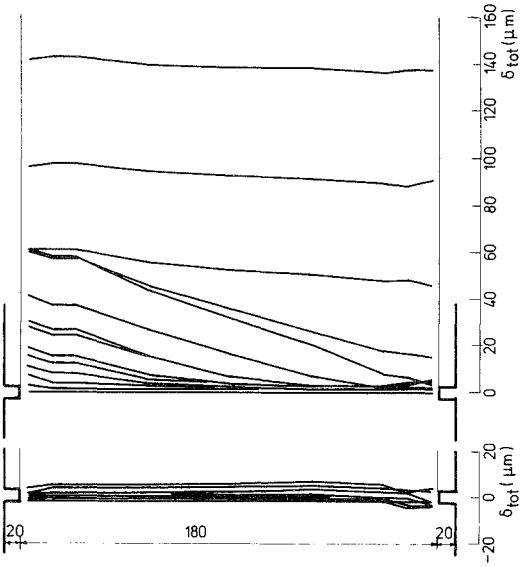

Fig. A4.5 Deformation distribution of the test of Fig. A4.4. Upper part: deformation at envelope stresses. Lower part: deformation at lower stress.

APPENDIX 5

Envelope curves

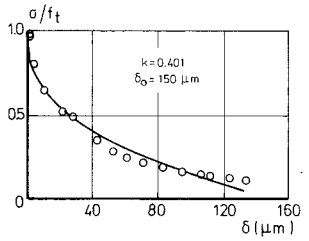

Fig. A5.1 Curve fitting of an envelope curve with $k = 0{,}401$ and $\delta_0 = 150$ μm.

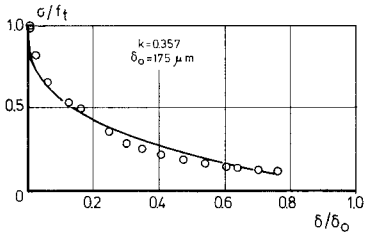

Fig. A5.2 Another example of an envelope curve with $k = 0{,}357$ and $\delta_0 = 175$ μm.

APPENDIX 6

Stress distribution of wide specimen during cyclic loading

Corresponds to strain distribution of Fig. 21.

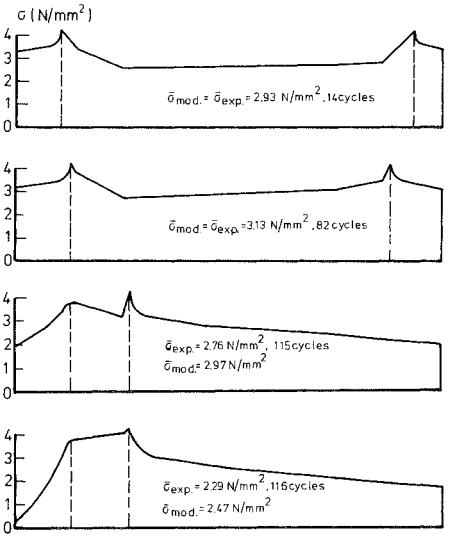

Fig. A6.1 ·Sequence of states of stress during repeated loading. This figure is a supplement to Fig. 28.